MDPI

Article

On Performance of Reconfigurable Intelligent Surface Communication System in Different Fading models

Siye Wang [1,†]*, Yeqin Huang [2,†] and Yong Yang [3,†]

† School of Arificial Intelligence, Beijing Univ. of Posts and Telecom.
[1] wsy@bupt.edu.cn
[2] yqhuangst@bupt.edu.cn
[3] YangYong.cn@outlook.com
* Correspondence: wsy@bupt.edu.cn.
† Current address: 10 Xitucheng Rd., Haidian District, Beijing, 100876 CHINA.

Abstract: In this paper, we develop a unified approach for evaluating the performance of a reconfigurable intelligent surface(RIS) wireless communication system in a generalized fading environment. We analyze the performance of average outage probability, symbol error rate, and ergodic capacity by deriving approximate expressions based on the Edgeworth series. The high signal-to-noise ratio regime is also discussed: Using the Cramér's large deviation principle, we get asymptotic expressions for these performances. Finally, we validate the accuracy by simulations of the mathematical results for various fading environments.

Keywords: reconfigurable intelligent rurface; channel fading; moment-based

1. Introduction

With the entry into the 5G\6G area, the number of networked devices and data transmission requirements have undergone significant changes [1]. A recently proposed new technology, reconfigurable intelligent surface (RIS), can be used to build smart radio environments, which are expected to enhance the quality of service of wireless communication systems [2–5]. The RIS is a man-made surface built with electromagnetic (EM) materials, with integrated electronics and a large number of reflective elements [6], which can be integrated into the infrastructure to reflect the signal for signal propagation. RIS uses optical properties to propagate the signal and does not involve active devices. Compared with traditional devices such as relays, it can transmit signals in a low-energy and low-cost manner. Meanwhile, due to the use of reflection for signal transmission, the transmission signal of RIS avoids encoding and decoding processing, reducing the difficulty of system design [7]. Thus, RIS is a great potential way in improving the performance of communication systems in 5G\6G wireless networks.

Traditional relay generally has two working modes, full-duplex (FD) mode and half-duplex (HD) mode, of which the two-way full-duplex transmission mode can achieve higher resource utilization by sharing time-frequency resources, thereby obtaining higher wireless system throughput [8–11]. FD increases the complexity of the system design while increasing system throughput—the FD operating mode introduces self-interference, and even when self-interference cancellation (SIC) techniques are used, there is residual self-interference (SI), and residual SI degrades the performance of FD wireless communication systems. There are two common processing methods for relaying signals, amplify-and-forward (AF) and decode-and-forward (DF). For RIS, in scenarios where it acts as a relay, its forwarding method can be regarded as an AF with an amplification factor of 1 [6] because it avoids the use of active devices to reduce energy consumption and uses reflections for signal propagation.

Due to the non-ideal nature of the propagation environment, the wireless communication system will be affected by fading and shadowing during signal propagation [12].

Citation: Wang, S.; Yeqin, H.; Yong, Y. On Performance of Reconfigurable Intelligent Surface Communication System in Different Fading models. *Appl. Sci.* **2022**, *1*, 0. https://doi.org/

Received:
Accepted:
Published:

These influencing factors are usually modeled by composite fading channels during system modeling. The most common composite fading models are Rayleigh-lognormal (RL) and Nakagami-lognormal (NL) distribution. However, under these complex fading models, it is complicated to obtain closed-form results when using indicators such as outage probability (OP), symbol error rate (SER), and channel capacity (CC) for performance analysis [13]. Therefore, some new composite models have been proposed to approximate these two mainstream models, including the Suzuki distribution, the K and generalized-K (KG) distributions, the G-distribution, and the Gamma distribution [14–18]. These models use mathematical methods such as the Gauss-Legendre integration to approximate the first two models, simplifying performance analysis.

The application of RIS-assisted wireless communication in communication systems has been studied in various fading scenarios. In [19], the ergodic rate of RIS-assisted systems under Rice fading was studied. RIS in the Device-to-Device(D2D) communication scenario by setting the phase and deployment location to reduce the interference caused by the shared spectrum of the cellular network was analyzed in [20]. [21] analyzed various indicators of point-to-point Nakagami fading channel and RIS-assisted transmission with phase error and verified the similarity in performance between the two. In [22], the bit error rate of a transmission system using RIS-assisted non-orthogonal multiple access (NOMA) was analyzed. The performance analysis results of wireless communication system transmission between RIS and relay under Rayleigh fading conditions were investigated in [23], showing that RIS and relay can be jointly optimized.

As an alternative to trunking in 5G\6G wireless networks, RIS can perform similar functions to relaying. In recent reports, the performance of wireless communication systems that use RIS in different ways of working, including comparing performance with relay networks, has been investigated. In [24], the scenario in which two devices use a RIS to communicate with each other in FD mode was studied, and the energy efficiency (EE) was maximized in the presence of SI by jointly optimizing the reflection coefficient matrix and the transmission power of the device. [25] considered the fairness of the multi-user two-way full-duplex wireless communication network that uses RIS for communication, and the reflection coefficient of RIS and the signal precoding matrix of the transmitting base station were jointly optimized to obtain optimal performance. RIS-assisted underwater optical communication system using the DF forwarding protocol was studied in [26]. The performance analysis of the RIS-assisted two-way half-duplex communication system was implemented in [27], and the correlation between the number of RIS reflective elements and the system performance indicators such as OP was obtained. In [28], the comparison results of the one-way half-duplex RIS communication system and one-way half-duplex relay system in terms of ergodic capacity and other indicators were provided. In [7], the OP and the SER of the RIS auxiliary communication system under the decline of Rayleigh were theoretically analyzed and numerically verified, and the performance was compared with the traditional relay system, which proved that RIS can obtain better performance than the traditional relay.

As pointed out in the previous discussion, the RIS-assisted communication system has been studied under various fading conditions. These studies use different mathematical methods to deal with non-closed solutions for composite fading models in the process of analysis, and there is no unified analysis and comparison. In this letter, considering a variety of fading conditions, we combine some classical mathematical theories to obtain a performance analysis method suitable for multiple fading channels, and use this method to analyze the performance indicators under multiple fading conditions, and at the same time verify the correctness of the theoretical method by simulation under multiple channel fading conditions. Considering system performance, the operating mode of RIS uses the bidirectional full-duplex operating mode in [7]. The contributions of this letter are as follows:

1. We consider a two-way full-duplex wireless communication system that uses RIS to replace traditional relay for signal forwarding to achieve signal transmission between

terminals. RIS adopts the AF mode of operation and takes into account non-ideal conditions, i.e. the presence of self-interfering transmissions.

2. We use the Edgeworth expansion theory and moment estimation method to derive the general expression of RIS-assisted full-duplex two-way wireless communication system under various fading channels in terms of OP, SER, etc.

3. The obtained results under various fading conditions are verified by Monte Carlo simulations. For RIS, different numbers of reflective elements are considered, and different modulation schemes are considered for symbol error rate. The feasibility of the proposed theoretical method is proved by theoretical results and simulation results.

We organize the rest of this paper as follows: Section II introduces the two-way full-duplex RIS (TW-FD-RIS) system model and the signal model. Section III deduces the theoretical results of general outage probability under independently identical distribution and independent but not identically distributed conditions. Section IV derives theoretical results for the average symbol error rate and ergodic rate. Section V shows the analysis results of theoretical and simulation verification of each performance index under different conditions. Finally, section VI is a summary of the full text.

2. System Model

We consider a TW-FD-RIS wireless communication system, whose model is presented in Fig. 1. A and B are two terminals, and due to the influence of factors such as fading and shadowing, the direct link between A and B is assumed to not exist and can only exchange information through a RIS. Each terminal is equipped with two transceiver antennas for sending signals to RIS and receiving forwarded signals from RIS. Since it is a two-way full-duplex wireless communication, there will be SI between the transceiver antennas. RIS has N reflective elements, and each terminal and each reflecting element will have a channel, with the fading coefficient between the terminal and the n-th reflective element represented by $h_{A,n}$, $h_{n,A}$, $g_{n,B}$, $g_{B,n}$. Considering the reciprocity of the channels, $h_{A,n}$, $h_{n,A}$ are represented by $h_{A,n}$, and $g_{n,B}$, $g_{B,n}$ are represented by $g_{n,B}$.

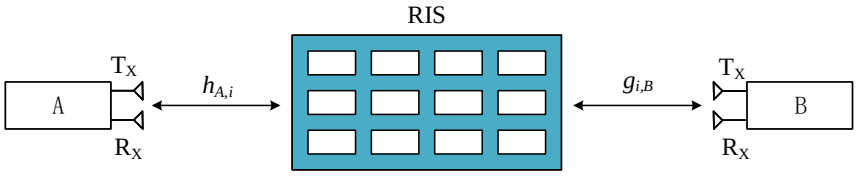

Figure 1. Illustration of the TW-FD-RIS system.

Considering the symmetry of the transmission, we only analyze the transmission signal from A to B. From [7], the instantaneous signal-to-interference-plus-noise ratio at the receiver B in the system is

$$\gamma = \frac{\left|\sum_{n=1}^{N} a_n b_n\right|^2 P_A}{X_B}, \tag{1}$$

where a_n, b_n are the channel gains for the send channel and receive channel, respectively.

There are several common fading channel models applied in Wireless communication systems. In the construction dense scene, there is usually no direct path between the terminal devices, and the wireless signal is transmitted and received by means of reflection, refraction, diffraction, where channel uses Rayleigh fading to model; if there is a direct path and reflection or diffraction paths between the terminals for signal transmission, Rice fading is generally used to model the channel; Weibull fading is suitable for small-scale fading vehicle-to-vehicle communication and multi-hop relay system communication scenarios; Nakagami-m fading was originally proposed to model fast-fading channels in the ionosphere and stratosphere, and later studies found that it was also suitable for land mobile communication channels, and could better match actual test results than Rayleigh and Rice channels. Table 1 gives the probability density function (pdf) of the channel gain in common

fading models mentioned above. Due to the difficulty of calculating the integrals using these probability density functions, the exact closed form of the cumulative probability distribution functions of $\sum_{n=1}^{N} a_n b_n$ always does not exists. To circumvent this difficulty, one shall use some methods to approximate the probability of the distributions. For instance, [27,29] proposed a moment matching technique, i.e., to use a gamma distribution to approximate the double Rayleigh distribution. Note that it only has freedom of two parameters in their modules, and hence it cannot be used in an arbitrary channel. The parameter α and θ in a Gamma distribution determine its expected value and variance, which measure its mean and dispersion. In statistics, higher-order moments like skewness and kurtosis are also often used to estimate a distribution. Some papers like [30,31] use the moments or moment generating functions to approximate such a random variable.

Note that the numerator in formula (1) has a term where independent random variables are summed up, and hence another classical technique: Feller's central limit theorem[32] can be used. However, Berry-Esseen bound[33,34] state that the converge rate of the central limit theorem is of size $\mathcal{O}(N^{-1/2})$, which is too slow. To accelerate the rate of convergence, one shall use a higher-order moment-based expansions for probability densities, which is called the Edgeworth expansion.

In this paper, we will use the Edgeworth expansion to approximate the distribution of formula (1) and then analysis the performance of the system based on the approximation. Table 2 gives the probability density function (pdf) and raw moments of the channel gain in common fading models. Clearly, for any fading types in table 1 and 2, the α-th moment are finite for any real $\alpha > 0$ (and hence the formula in theorem 1 and 2 are valid).

Table 1. Fading Types and their pdf.

Fading Type	**probability density of $\|h\|$(channel gains)**
Rayleigh	$\frac{x}{\sigma^2}\mathrm{e}^{-\frac{x^2}{2\sigma^2}}\mathbf{1}_{(x>0)}$
Nakagami-m	$\frac{2m^m}{\Gamma(m)\Omega^m}x^{2m-1}\mathrm{e}^{-\frac{mx^2}{\Omega}}\mathbf{1}_{(x>0)}$
Rician	$\frac{2(K+1)x}{\Omega}\mathrm{e}^{-K-\frac{K+1}{\Omega}x^2}I_0\left(2\sqrt{\frac{K(K+1)}{\Omega}}x\right)$
Weibull	$2k(\frac{\beta}{\Omega})^k x^{2k-1}\mathrm{e}^{-\left(\frac{x^2\beta}{\Omega}\right)^k}, \beta=\Gamma(1+\frac{1}{k})$
Generalized Γ	$\frac{2p(\beta/\omega)^d}{\Gamma(d/p)}x^{2d-1}\mathrm{e}^{-\left(\frac{x^2\beta}{\Omega}\right)^p}, \beta=\frac{\Gamma((d+1)/p)}{\Gamma(d/p)}$
Squared $\kappa-\mu$	$\frac{2\mu(1+\kappa)^{\frac{\mu+1}{2}}x^\mu}{\Omega^{\frac{\mu+1}{2}}\kappa^{\frac{\mu-1}{2}}\mathrm{e}^{\mu\kappa}}\mathrm{e}^{-\frac{(1+\kappa)\mu x^2}{\Omega}}I_{\mu-1}(2\mu\sqrt{\frac{\kappa(1+\kappa)}{\Omega}}x)$

Table 2. Fading Types and their moments.

Fading Type	**α-th moment($\mathbb{E}\|h\|^\alpha$)**
Rayleigh	$\sigma^\alpha 2^{\alpha/2}\Gamma\left(1+\frac{\alpha}{2}\right)$
Nakagami-m	$\frac{\Gamma(\frac{\alpha}{2}+m)}{(\frac{m}{\Omega})^{\alpha/2}\Gamma(m)}$
Rician	$\frac{\Gamma(1+\frac{\alpha}{2})\,{}_1F_1(-\frac{\alpha}{2};1;-K)}{(\frac{1+K}{\Omega})^{\alpha/2}}$
Weibull	$(\frac{\beta}{\Omega})^{-\alpha/2}\Gamma(1+\frac{\alpha}{2k})$
Generalized Gamma	$(\frac{\beta}{\Omega})^{-\alpha/2}\frac{\Gamma(\frac{\alpha+2d}{2p})}{\Gamma(d/p)}$
Squared $\kappa-\mu$	$\frac{\Omega^{\frac{\alpha}{2}}\Gamma(\mu+\frac{\alpha}{2})\mathrm{e}^{-\kappa\mu}}{\mu(1+\kappa)\Gamma(\mu)}\,{}_1F_1(\frac{\alpha}{2}+\mu;\mu;\kappa\mu)$

Notations: We use $\Phi(\cdot)$ and $\varphi(\cdot)$ to denote the cumulative distribution function and the probability density function of the standard normal distribution, respectively. $\mathcal{P}$

and $\mathbb{E}$ denotes the probability measure and the expectation operator, respectively. The (probabilist's) Hermite polynomial of order n is denoted as $H_{e_n}(\cdot)$. $\Gamma(\cdot)$ denotes the gamma function, and $I_\nu(\cdot)$ denotes the modified Bessel functions of the first kind. The functions of the form ${}_1F_1(a;b;z)$ denotes the confluent hypergeometric functions of the first kind.

3. Outage Probability

The average outage probability is given by

$$\mathcal{P}_{\text{out}} := \mathcal{P}(\gamma < \gamma_{\text{th}}) = \mathcal{P}\Big(\sum_{n=1}^{N} a_n b_n < \sqrt{\frac{X_{\text{B}}\gamma_{\text{th}}}{P_{\text{A}}}} \Big), \tag{2}$$

where γ_{th} is threshold of SINR, and a_{n}, b_{n} are the gains of the channel between terminal A and n-th reflection element in RIS, between n-th reflection element in RIS and terminal B, respectively.

3.1. i.i.d. Channel Coefficients

Theorem 1. *If the channel gains $a_1, \cdots, a_N$ and $b_1, \cdots, b_N$ are i.i.d r.v's from distribution F_A and F_B, respectively. Futhermore, assume that $\sigma^2 = \text{var}(a_1 b_1) > 0$ and*

$$\mathbb{E}|a_1 b_1|^r < \infty, \quad \overline{\lim_{|t|\to\infty}} |\mathbb{E}\exp(\text{i} a_1 b_1 t)| < 1. \tag{3}$$

Then the outage probability in (2) can be approximate as

$$G(x) := \Phi(x) - \sum_{k=3}^{r} N^{-\frac{k-2}{2}} \frac{\kappa_k}{\sigma^k k!} H_{e_{k-1}}(x)\varphi(x), \tag{4}$$

where $x = \frac{\sqrt{\frac{X_{\text{B}}\gamma_{\text{th}}}{P_{\text{A}}}} - N\kappa_1}{\sqrt{N}\sigma}$ and the Hermite polynomial $H_{e_n}(x)$ of order n on $\mathbb{R}$ is defined as

$$H_{e_n}(x) = (-1)^n \text{e}^{x^2/2} \big(\frac{\text{d}}{\text{d}x}\big)^n \text{e}^{-x^2/2}. \tag{5}$$

$\Phi(\cdot)$ and $\varphi(\cdot)$ is the cdf and pdf of standard normal distribution, respectively. The cumulants $\kappa_p's$ in (4) is given by

$$\kappa_p = p! \sum (-1)^{s_p - 1}(s_p - 1)! \prod_{j=1}^{p} \frac{1}{k_j!} \Big(\frac{\mathbb{E}(a_1 b_1)^j}{j!} \Big)^{k_j}, \tag{6}$$

where $s_p = k_1 + \cdots + k_p$ and where the summation is running over all non-negative integer tuples $(k_1, \cdots, k_p)$ such that $k_1 + 2k_2 + \cdots + pk_p = p$. The error incurred by approximating the outage probability of (4) is of size $\mathcal{O}(N^{-\frac{r-2}{2}})$.

According to the classical Edgeworth's expansion, this result is trivial. Hence Theorem 1 follows directly by the main result (equation 4) in [35](1982). One could use the characteristic function, Lindeberg device, or Stein's method to prove it. About these mathematical proofs, please refer to [35,36].

Remark 1. *The first few formula for equation (6) is*

$$\begin{aligned} \kappa_1 &= \mathbb{E}a_1 b_1, \quad \kappa_2 = \mathbb{E}a_1^2 b_1^2 - \kappa_1^2, \\ \kappa_3 &= \mathbb{E}a_1^3 b_1^3 - 3\kappa_1 \mathbb{E}a_1^2 b_1^2 + 2\kappa_1^3, \\ \kappa_4 &= \mathbb{E}a_1^4 b_1^4 - 4\kappa_1 \mathbb{E}a_1^3 b_1^3 - 3(\mathbb{E}a_1^2 b_1^2)^2 + 12\kappa_1^2 \mathbb{E}a_1^2 b_1^2 - 6\kappa_1^4. \end{aligned} \tag{7}$$

Remark 2. *It may be difficult to use formula (6) in programming, one could use the following recurrence relations to simplify the calculation:*

$$\kappa_p = \mathbb{E}(a_1^p b_1^p) - \sum_{k=1}^{p-1} \binom{p-1}{k-1} \kappa_k \mathbb{E}(a_1^{p-k} b_1^{p-k}). \tag{8}$$

The Cramér's rule in linear algebra yields an expression

$$\kappa_p = \begin{vmatrix} \mathbb{E}(a_1 b_1) & \frac{\mathbb{E}(a_1^2 b_1^2)}{2} & \cdots & \frac{\mathbb{E}(a_1^{p-1} b_1^{p-1})}{(p-1)!} & \frac{\mathbb{E}(a_1^p b_1^p)}{p!} \\ 1 & \mathbb{E}(a_1 b_1) & \cdots & \frac{\mathbb{E}(a_1^{p-2} b_1^{p-2})}{(p-2)!} & \frac{\mathbb{E}(a_1^{p-1} b_1^{p-1})}{(p-1)!} \\ \vdots & \vdots & \ddots & \vdots & \vdots \\ 0 & 0 & \cdots & \mathbb{E}(a_1 b_1) & \frac{\mathbb{E}(a_1^2 b_1^2)}{2} \\ 0 & 0 & \cdots & 1 & \mathbb{E}(a_1 b_1) \end{vmatrix}. \tag{9}$$

Note that this is a determinant of a Toeplitz matrix, one could also apply some algorithm in the linear algebra to solve it, for instance, the Levinson's algorithm[37].

Remark 3. *In theorem 1, when $r = 5$,the result is given by*

$$\begin{aligned} G(x) = \Phi(x) - \Bigg[& \frac{\kappa_3}{\sqrt{N}\sigma^3 3!}(x^2-1) + \frac{\kappa_4}{N\sigma^4 4!}(x^3-3x) \\ & + \frac{\kappa_5}{N\sqrt{N}\sigma^5 5!}(x^4-6x^2+3) \Bigg] \varphi(x). \end{aligned} \tag{10}$$

3.2. Non-identically distributed Channel Coefficient

Due to path loss, the scale parameter of the distribution of channel coefficients is determined by the geometrical position of the N reflecting elements. Hence, sometimes we cannot assume that the channel coefficients are i.i.d.. Our next step is to generalize the result to independent channel coefficients (which may not be identically distributed).

Theorem 2. *Let the channel coefficients $a_1, \cdots, a_n$ and $b_1, \cdots, b_n$ be independent random variables. Suppose*

$$\sigma^2 := \sum_{k=1}^{N} \operatorname{var}(a_k b_k) > 0, \quad \sum_{k=1}^{N} \mathbb{E}|a_k b_k|^r < \infty. \tag{11}$$

Let $x = (\sqrt{\frac{X_B \gamma_{th}}{P_A}} - \sum_{k=1}^{N} \mathbb{E} a_k b_k)/\sigma$ and

$$\kappa_p = p! \sum (-1)^{s_p - 1} (s_p - 1)! \sum_{k=1}^{N} \prod_{j=1}^{p} \frac{1}{k_j!} \left(\frac{\mathbb{E}(a_k b_k)^j}{j!} \right)^{k_j}, \tag{12}$$

where $s_p = k_1 + \cdots + k_p$ and where the summation is running over all non-negative integer tuples $(k_1, \cdots, k_p)$ such that $k_1 + 2k_2 + \cdots + pk_p = p$. Then the outage probability in (2) can be approximate as

$$G(x) := \Phi(x) - \sum \frac{\left(\frac{\kappa_3}{3!}\right)^{k_1} \cdots \left(\frac{\kappa_r}{r!}\right)^{k_{r-2}}}{\sigma^k k_1! \cdots k_{r-2}!} H_{e_{k-1}}(x) \varphi(x), \tag{13}$$

where $k = 3k_1 + \cdots + rk_{r-2}$ and where the summation runs over all collections of non-negative integer tuples $(k_1, \cdots, k_{r-2})$ that are not all zero and such that $k_1 + 2k_2 \cdots + (r-2)k_{r-2} \leq r-2$.

Theorem 2 is a direct consequence of Edgeworth's expansion in the non-identical situation. [38] has a detailed discussion on this problem of the one-dimension random variables. [36] studies the distribution norm and the rate of the convergence of these

expansions and has generalized the theorem in [38] to multi-dimension random vector sequences. Here, we shall only use the one-dim case of [36] in theorem 2.

Remark 4. *In theorem 2, when $r = 6$, $\sigma = 1$, the result is given by*

$$\begin{aligned} G(x) = \Phi(x) - \varphi(x)\Big[&\frac{\kappa_3}{3!}(x^2-1) + \frac{\kappa_4}{4!}(x^3-3x) \\ &+ \frac{\kappa_5}{5!}(x^4-6x^2+3) + \Big(\frac{\kappa_6}{6!} + \frac{\kappa_3^2}{2!3!^2}\Big)(x^5-10x^3+15x) \\ &+ \Big(\frac{\kappa_3\kappa_5}{3!5!} + \frac{\kappa_4^2}{2!4!^2}\Big)(x^7-21x^5+105x^3-105x) \\ &+ \frac{\kappa_3^3}{3!^4}(x^8-28x^6+210x^4-420x^2+105) \\ &+ \frac{\kappa_3^2\kappa_4}{2!3!^2 4!}(x^9-36x^7+378x^5-1260x^3+945x) \\ &+ \frac{\kappa_3^4}{4!3!^4}(x^{11}-55x^9+990x^7-6930x^5+17325x^3-10395x)\Big]. \end{aligned} \tag{14}$$

3.3. Asymptotic SNR

Here, we will consider the system performance under asymptotic snr, i.e, as snr $\to \infty$. At high snr, it is better to use the Cramér's large deviation principles[34,39–41] to approximate the distribution. The following lemma is the well known Cramér's large deviation principles, and [41,42] generalized it to independent random variable sequences.

Lemma 1 (Cramér's Large Deviation)**.** *Suppose an i.i.d. r.v. sequence $\{X_n\}_{n=1}^{\infty}$ where $\mathbb{E}X_1 = 0$, $\mathbb{E}X_1^2 = 1$, and $\exists t_0 > 0$, s.t.*

$$\mathbb{E}e^{t|X_1|} < \infty, \quad \forall 0 < t < t_0. \tag{15}$$

Put $S_n = \sum_{k=1}^{n} X_k$ be the partial sum of $\{X_n\}$. If $x > 0$, $x = o(\sqrt{n})$, as $n \to \infty$, then

$$\frac{\mathcal{P}(S_n < -\sqrt{n}x)}{\Phi(-x)} = \exp\Big(\frac{x^3}{\sqrt{n}}\lambda(\frac{x}{\sqrt{n}})\Big)\Big(1 + \mathcal{O}(\frac{1+x}{\sqrt{n}})\Big), \tag{16}$$

where $\lambda(z) = \sum_{k=0}^{\infty} a_k z^k$ is the Cramér's series, and a_k is determined by the first $(k+3)$-th order cumulants of X_1. For instance,

$$a_0 = \frac{\kappa_3}{6}, \quad a_1 = \frac{\kappa_4 - 3\kappa_3^2}{24}, \tag{17}$$

where κ_k is the k-th order cumulant of X_1.

At high snr, the SINR at the receiver becomes

$$\gamma = \frac{\left|\sum_{n=1}^{N} a_n b_n\right|^2 P_A}{X_B} = \frac{\left|\sum_{n=1}^{N} a_n b_n\right|^2 P_A}{k_B^2 P_B + \sigma_B^2} \to \frac{\left|\sum_{n=1}^{N} a_n b_n\right|^2}{k_B^2}, \quad \text{almost surely.} \tag{18}$$

Now, equation (4) becomes

$$G(x) \approx \Phi(x)\exp\Big(\frac{\kappa_3 x^3}{6\sqrt{N}} + \frac{(\kappa_4 - 3\kappa_3^2)x^4}{24N}\Big). \tag{19}$$

4. Average Symbol Error Rate and Ergodic Rate

4.1. Average Symbol Error Rate Analysis

The average symbol error rate at B in the system is given by

$$\mathrm{SER} = \alpha \mathbb{E}\, Q(\sqrt{\beta\gamma}), \tag{20}$$

where $Q(x) = \int_x^{+\infty} \varphi(u)\,\mathrm{d}u$ is the tail distribution function of the standard normal distribution.

Table 3. α and β in equation (20).

Modulation Type	α	β
BPSK	1	2
QPSK(4-QAM)	2	1
8-QAM	$4-\sqrt{2}$	3/7
9-QAM	8/3	3/8
16-QAM	3	1/5
27-QAM	$\frac{4}{9}-\frac{4\sqrt{3}}{9}$	3/26
64-QAM	7/2	1/21
256-QAM	15/4	1/85
1024-QAM	31/8	1/341

The constants α and β are depend on the modulation types. Table 3 gives these parameters in PSK and QAM modulations. Here, except for 2^m-ary QAM modulation, other types of QAM modulation may be used in some non-binary channel codings, including the non-binary LDPC Codes (over Galois Field $\mathbb{F}_{p^r}$)[43,44], non-binary Polar Codes[45,46], etc.

Theorem 3. *The average symbol error rate of this system is approximated as*

$$\mathrm{SER} \approx \frac{\alpha\sqrt{\pi}}{4M} \sum_{m=1}^{M} \frac{\sqrt{1-\phi_m^2}}{\sqrt{\ln(2/(\phi_m+1))}} F_\gamma\Big(\frac{\ln(2/(\phi_m+1))}{\beta/2}\Big), \tag{21}$$

where $\phi_m = \cos(\frac{2m-1}{2M}\pi)$ *and* M *is the trade-off parameter of the accuracy. The distribution function* F_γ *is approximated by Theorem 1 and Theorem 2 as follows:*

$$F_\gamma(y) = \begin{cases} G\Big(\frac{\sqrt{\frac{X_B y}{P_A}} - N\kappa_1}{\sqrt{N}\sigma}\Big), & \textit{in Thm. 1,} \\ G\Big((\sqrt{\frac{X_B y}{P_A}} - \sum_{k=1}^{N} \mathbb{E}a_k b_k)/\sigma\Big), & \textit{in Thm. 2.} \end{cases} \tag{22}$$

Proof. By definition and Fubini's theorem, we have

$$\begin{aligned} \mathrm{SER} &= \alpha\mathbb{E}Q(\sqrt{\beta\gamma}) = \int_0^\infty \alpha \int_{\sqrt{\beta x}}^\infty \frac{1}{\sqrt{2\pi}} \mathrm{e}^{-\frac{t^2}{2}}\,\mathrm{d}t\,\mathrm{d}F_\gamma(x) \\ &= \frac{\alpha}{\sqrt{2\pi}} \int_0^\infty \mathrm{e}^{-\frac{t^2}{2}} \int_0^{\frac{t^2}{\beta}} \mathrm{d}F_\gamma(x)\,\mathrm{d}t = \frac{\alpha}{\sqrt{2\pi}} \int_0^\infty F_\gamma(t^2/\beta)\mathrm{e}^{-t^2/2}\,\mathrm{d}t. \end{aligned} \tag{23}$$

Changing variables $u = 2\mathrm{e}^{-t^2/2} - 1$ and then using the Chebyshev-Gauss quadrature gives

$$\mathrm{SER} = \frac{\alpha}{4\sqrt{\pi}} \int_{-1}^{1} F_\gamma\Big(\frac{\ln\frac{2}{u+1}}{\beta/2}\Big) \frac{\mathrm{d}u}{\sqrt{\ln\frac{2}{u+1}}} = \frac{\alpha}{4\sqrt{\pi}} \frac{\pi}{M} \sum_{m=1}^{M} \frac{\sqrt{1-\phi_m^2}}{\sqrt{\ln\frac{2}{\phi_m+1}}} F_\gamma\Big(\frac{\ln\frac{2}{\phi_m+1}}{\beta/2}\Big), \tag{24}$$

which proves the desired result. □

4.2. Ergodic Rate Analysis

In what follows, we will consider getting an expression of the ergodic rate. Due to the computational difficulty of deriving the exact closed-form expression, and for the sake of simplicity, we will apply the Chebyshev-Gauss quadrature to simplify our analysis.

Theorem 4. *The ergodic rate is given by*

$$\mathrm{ER} \approx \frac{\pi}{M} \sum_{m=1}^{M} \Big[1 - F_{\gamma}(\frac{1-\phi_m}{1+\phi_m})\Big] \sqrt{\frac{1-\phi_m}{1+\phi_m}}, \tag{25}$$

where $\phi_m = \cos(\frac{2m-1}{2M}\pi)$, $M > 0$ *and where* $F_{\gamma}(\cdot)$ *is same as equation (22).*

Proof. Using the Fubini's theorem, we get

$$\begin{aligned} \mathrm{ER} := \mathbb{E}\ln(1+\gamma) &= \int_0^{\infty} \ln(1+x)\, \mathrm{d}F_{\gamma}(x) \\ &= \int_0^{\infty} \int_0^{x} \frac{1}{1+y}\, \mathrm{d}y\, \mathrm{d}F_{\gamma}(x) \\ &= \int_0^{\infty} \frac{1}{1+y} \int_y^{\infty} \mathrm{d}F_{\gamma}(x)\, \mathrm{d}y \\ &= \int_0^{\infty} \frac{1-F_{\gamma}(y)}{1+y}\, \mathrm{d}y. \end{aligned} \tag{26}$$

Changing variables $u = \frac{1-y}{1+y}$ and then using the Chebyshev-Gauss quadrature gives

$$\begin{aligned} \mathrm{ER} &= \int_{-1}^{1} \Big[1 - F_{\gamma}(\frac{1-t}{1+t})\Big] \frac{\mathrm{d}t}{1+t} \\ &\approx \frac{\pi}{M} \sum_{m=1}^{M} \Big[1 - F_{\gamma}(\frac{1-\phi_m}{1+\phi_m})\Big] \sqrt{\frac{1-\phi_m}{1+\phi_m}}, \end{aligned} \tag{27}$$

and hence the theorem. □

5. Numerical Results

In the numerical parts, we both use the six-order ($r = 6$) expansion in theorem 1 and 2. In the simulation and theoretical models, we set parameter $X_{\mathrm{B}} = k_{\mathrm{B}}^2 P_{\mathrm{B}} + \sigma_{\mathrm{B}}^2$, where $k_{\mathrm{B}}^2 = 10^{-2}$, $P_{\mathrm{A}} = P_{\mathrm{B}} = P$, $\mathrm{snr} = P/\sigma_{\mathrm{B}}^2$, and $\gamma_{\mathrm{th}} = 1$. We use the Monte-Carlo simulation to verify our mathematical results. All the figures show the corresponding system performance versus the average snr.

Fig. 2 to 4 show the average outage probability of the system in different fading channels versus the average SNR with i.i.d case, while Fig. 5 shows the non-identical case. In Fig. 2, we set the channel fading a_n and b_n to be both independent and identically Rayleigh distributed with shape parameter $\sigma = \frac{1}{\sqrt{2}}$. In Fig. 3, we set the channel fading a_n and b_n to be both independent and identically Rician distributed with parameter $K = 5$ and $\Omega = 1$. Fig. 4, we set the channel fading a_n and b_n to be both independent and identically Weibull distributed with parameter $\Omega = 1/2$ and $k = 5$. In Fig. 5, we assume that $N = 4$. For the Rician fading, we set four different parameter to the channel gains: $a_1, b_1 \sim$ Rician$(K = 5, \Omega = 1)$, $a_2, b_2 \sim$ Rician$(K = 6, \Omega = 1)$, $a_3, b_3 \sim$ Rician$(K = 5, \Omega = 1.5)$, $a_4, b_4 \sim$ Rician$(K = 6, \Omega = 1.5)$. For the Weibull fading, we also set four different channels, their parameters are: $a_1, b_1 \sim$ Weibull$(\Omega = 0.5, k = 5)$, $a_2, b_2 \sim$ Weibull$(\Omega = 1, k = 5)$, $a_3, b_3 \sim$ Weibull$(\Omega = 0.5, k = 6)$, and $a_4, b_4 \sim$ Weibull$(\Omega = 1, k = 5)$.

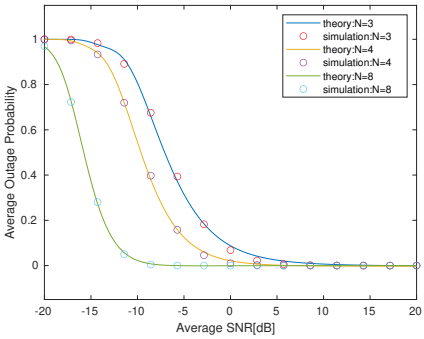

Figure 2. Average outage probability versus the average snr, all the channels are Rayleigh fading, with parameter $\sigma = 1/\sqrt{2}$.

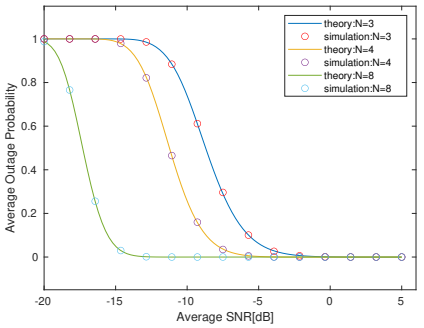

Figure 3. Average outage probability versus the average snr, all the channels are Rician fading, with parameter $K = 5, \Omega = 1$.

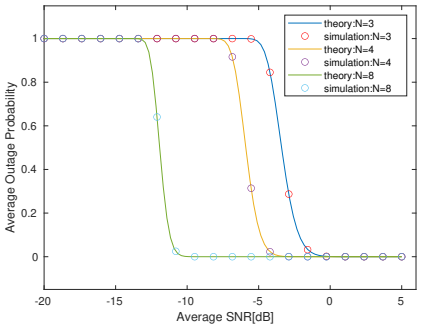

Figure 4. Average outage probability versus the average snr, all the channels are Weibull fading, with parameter $\Omega = 0.5, k = 5$.

As seen from the Fig. 2 to 5, the average outage probability in all the fading channels is lower with the higher average SNRs. In low SNR, channels that use more reflection elements in RIS achieve lower average outage probability and in high SNR, almost closed. It also can be observed that the theory derived results are similar to the Monte-Carlo simulation results, which proves the validness of the proposed method.

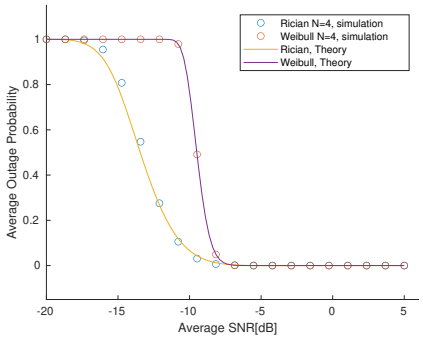

Figure 5. Average outage probability versus the average snr, for four channels with different parameters.

In Fig. 6 and 7, we simulate and verify the theorem 3. In Fig. 6 and 7, we choose the parameter $k_B^2 = 10^{-4}$, and the parameter $M = 40$ in Chebyshev-Gauss quadrature. We choose the Rician and Weibull distributed fading same as Fig. 3 and 4., and tested for the BPSK, 4-QAM, and 8-QAM modulation, respectively.

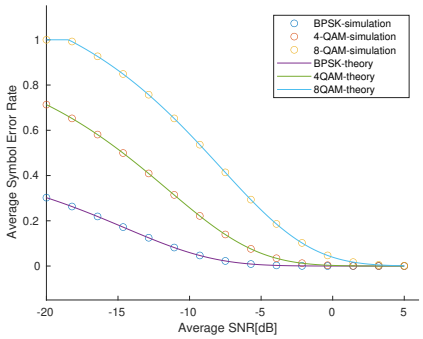

Figure 6. Average Symbol Error Rate for four Rician fading channel, with parameter $K = 5$, $\Omega = 1$.

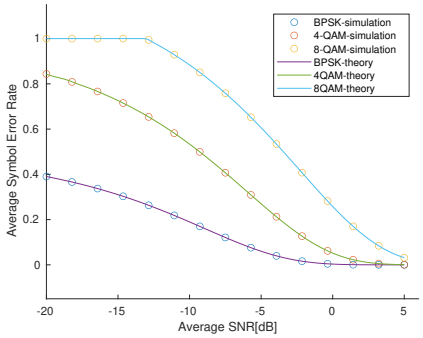

Figure 7. Average Symbol Error Rate for four Weibull fading channel, with parameter $\Omega = 0.5$, $k = 5$.

As Fig. 6 and 7 show, different modulation obtains different average symbol rates under the same SNR, and they all get lower symbol error rate with the SNRs are higher. More importantly, even transmission signals are modulated with different types, their theory results also meet the simulation results.

In Fig. 8 and 9, we simulate and verify the theorem 4. Here we used the same parameter in Fig. 6 and 7, respectively. With the SNRs being higher and more elements used in RIS, whether Rician fading or Weibull fading system achieves higher ergodic rate.

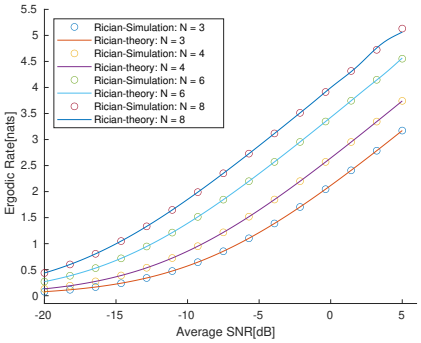

Figure 8. Ergodic Rate for Rician Fading channels, with parameter $K = 5$, $\Omega = 1$.

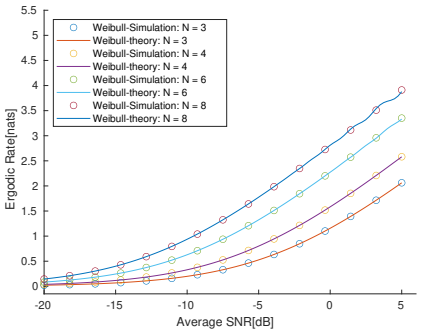

Figure 9. Ergodic Rate for Weibull Fading channels, with parameter $\Omega = 0.5$, $k = 5$.

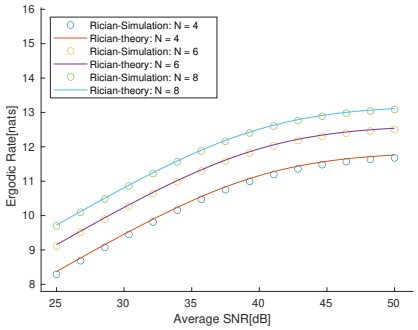

Figure 10. Asymptotic Ergodic Rate for Rician Fading channels, with parameter $K = 5$, $\Omega = 1$.

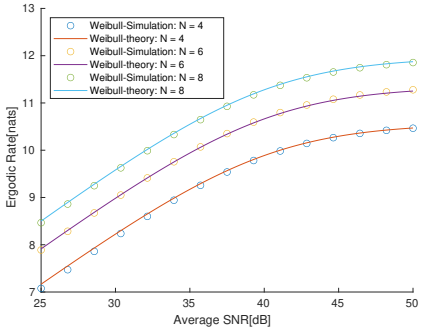

Figure 11. Asymptotic Ergodic Rate for Weibull Fading channels, with parameter $\Omega = 0.5$, $k = 5$.

Fig. 10 and 11 plots the asymptotic behaviours as snr $\to \infty$.

6. Conclusion

This paper explores an Edgeworth expansion method and a Cramér's large deviation method to approximate the distributions in the reconfigurable intelligent surface network. We started with the foundation of estimating distributions by Edgeworth expansion; then from there, we derived the system performance expressions, including the outage probability, symbol error rate, and ergodic rate. Moreover, we have used the large deviation principle to estimate the asymptotic snr behavior. From above, there is no need of calculating any integrals to analyze the system performance, the only thing we used is the moments of the channel gains. Hence, we proposed a unified moment-based method for analyzing the performance of the RIS network. The Monte-Carlo simulations indeed show that the proposed method has good finite behavior, which experimentally confirms our method.

Author Contributions: investigation, methodology and supervision: Siye Wang; simulation and validation, Yeqin Huang; conceptualization and formal analysis, Yong Yang; writing—original draft preparation and visualization, Yeqin Huang and Yong Yang; writing—review and editing, Siye Wang. All authors have read and agreed to the published version of the manuscript.

Funding: This research received no external funding.

Institutional Review Board Statement: Not applicable.

Data Availability Statement: The source files are free under a BSD license . Our data and matlab codes can be found at https://bupt-yy.github.io/notes/Miscellaneous. In the matlab codes, probHermiteH.m uses the Horner's algorithm to calculates the Hermite polynomials. calcCumulantByMoment.m calculates the equation (6). Others are the numerical parts that simulate and verify our results.

Acknowledgments: The authors would like to thank a referee for several insightful comments and suggestions which helped us to improve the paper.

Conflicts of Interest: The authors declare that they have no conflict of interests.

Abbreviations

The following abbreviations are used in this manuscript:

FD	Full-Duplex
pdf	Probability Density Function
cdf	cumulative (probability measure) distribution function
ch.f.	Characteristic Function
r.v.	Random Variable
i.i.d.	Independent and Identically Distributed
AF	Amplify-and-forward
ER	Ergodic Rate
OP	Outage Probability
SNR	Signal-to-noise Ratio
SINR	Signal-to-interference-plus-noise ratio
BER	Bit Error Rate
SER	Symbol Error Rate
RIS	Reconfigurable Intelligent Surface
QAM	Quadrature Amplitude Modulation
PSK	Phase-shift keying
LDPC	Low-density Parity Check Codes
NOMA	Nonorthogonal Multiple Access

References

1. Boccardi, F.; Heath, R.W.; Lozano, A.; Marzetta, T.L.; Popovski, P. Five disruptive technology directions for 5G. *IEEE Communications Magazine* **2014**, *52*, 74–80. doi:10.1109/MCOM.2014.6736746.

2. Wu, Q.; Zhang, R. Intelligent Reflecting Surface Enhanced Wireless Network: Joint Active and Passive Beamforming Design. In Proceedings of the 2018 IEEE Global Communications Conference (GLOBECOM), 2018, pp. 1–6. doi:10.1109/GLOCOM.2018.8647620.
3. Wu, Q.; Zhang, R. Intelligent Reflecting Surface Enhanced Wireless Network via Joint Active and Passive Beamforming. *IEEE Transactions on Wireless Communications* **2019**, *18*, 5394–5409. doi:10.1109/TWC.2019.2936025.
4. Huang, C.; Zappone, A.; Debbah, M.; Yuen, C. Achievable Rate Maximization by Passive Intelligent Mirrors. In Proceedings of the 2018 IEEE International Conference on Acoustics, Speech and Signal Processing (ICASSP), 2018, pp. 3714–3718. doi:10.1109/ICASSP.2018.8461496.
5. Tan, X.; Sun, Z.; Koutsonikolas, D.; Jornet, J.M. Enabling Indoor Mobile Millimeter-wave Networks Based on Smart Reflect-arrays. In Proceedings of the IEEE INFOCOM 2018 - IEEE Conference on Computer Communications, 2018, pp. 270–278. doi:10.1109/INFOCOM.2018.8485924.
6. Basar, E.; Di Renzo, M.; De Rosny, J.; Debbah, M.; Alouini, M.S.; Zhang, R. Wireless Communications Through Reconfigurable Intelligent Surfaces. *IEEE Access* **2019**, *7*, 116753–116773. doi:10.1109/ACCESS.2019.2935192.
7. Nguyen, B.C.; Hoang, T.M.; Dung, L.T.; Kim, T. On Performance of Two-Way Full-Duplex Communication System With Reconfigurable Intelligent Surface. *IEEE Access* **2021**, *9*, 81274–81285. doi:10.1109/ACCESS.2021.3086067.
8. Kim, D.; Lee, H.; Hong, D. A Survey of In-Band Full-Duplex Transmission: From the Perspective of PHY and MAC Layers. *IEEE Communications Surveys Tutorials* **2015**, *17*, 2017–2046. doi:10.1109/COMST.2015.2403614.
9. Zhang, Z.; Long, K.; Vasilakos, A.V.; Hanzo, L. Full-Duplex Wireless Communications: Challenges, Solutions, and Future Research Directions. *Proceedings of the IEEE* **2016**, *104*, 1369–1409. doi:10.1109/JPROC.2015.2497203.
10. Khalili, A.; Mili, M.R.; Ng, D.W.K. Performance Trade-off Between Uplink and Downlink in Full-Duplex Communications. In Proceedings of the ICC 2020 - 2020 IEEE International Conference on Communications (ICC), 2020, pp. 1–6. doi:10.1109/ICC40277.2020.9148981.
11. Khalili, A.; Zarandi, S.; Rasti, M.; Hossain, E. Multi-Objective Optimization for Energy- and Spectral-Efficiency Tradeoff in In-Band Full-Duplex (IBFD) Communication. In Proceedings of the 2019 IEEE Global Communications Conference (GLOBECOM), 2019, pp. 1–6. doi:10.1109/GLOBECOM38437.2019.9013637.
12. Maseng, T. Digital communication over fading channels: a unified approach to performance analysis [Book Review]. *IEEE Communications Magazine* **2001**, *39*, 36–36. doi:10.1109/MCOM.2001.933432.
13. Sofotasios, P.C.; Freear, S. On the κ-μ/gamma composite distribution: A generalized multipath/shadowing fading model. In Proceedings of the 2011 SBMO/IEEE MTT-S International Microwave and Optoelectronics Conference (IMOC 2011). IEEE, 2011, pp. 390–394.
14. Suzuki, H. A Statistical Model for Urban Radio Propogation. *IEEE Transactions on Communications* **1977**, *25*, 673–680. doi:10.1109/TCOM.1977.1093888.
15. Abdi, A.; Kaveh, M. K distribution: An appropriate substitute for Rayleigh-lognormal distribution in fading-shadowing wireless channels. *Electronics Letters* **1998**, *34*, 851–852.
16. Shankar, P.M. Error rates in generalized shadowed fading channels. *Wireless personal communications* **2004**, *28*, 233–238.
17. Laourine, A.; Alouini, M.S.; Affes, S.; Stephenne, A. On the performance analysis of composite multipath/shadowing channels using the G-distribution. *IEEE Transactions on Communications* **2009**, *57*, 1162–1170. doi:10.1109/TCOMM.2009.04.070258.
18. Al-Ahmadi, S.; Yanikomeroglu, H. On the approximation of the generalized-K distribution by a gamma distribution for modeling composite fading channels. *IEEE Transactions on Wireless Communications* **2010**, *9*, 706–713. doi:10.1109/TWC.2010.02.081266.
19. Jung, M.; Saad, W.; Jang, Y.; Kong, G.; Choi, S. Performance analysis of large intelligent surfaces (LISs): Asymptotic data rate and channel hardening effects. *IEEE Transactions on Wireless Communications* **2020**, *19*, 2052–2065.
20. Chen, Y.; Ai, B.; Zhang, H.; Niu, Y.; Song, L.; Han, Z.; Vincent Poor, H. Reconfigurable Intelligent Surface Assisted Device-to-Device Communications. *IEEE Transactions on Wireless Communications* **2021**, *20*, 2792–2804. doi:10.1109/TWC.2020.3044302.
21. Badiu, M.A.; Coon, J.P. Communication Through a Large Reflecting Surface With Phase Errors. *IEEE Wireless Communications Letters* **2020**, *9*, 184–188. doi:10.1109/LWC.2019.2947445.
22. Thirumavalavan, V.C.; Jayaraman, T.S. BER Analysis of Reconfigurable Intelligent Surface Assisted Downlink Power Domain NOMA System. In Proceedings of the 2020 International Conference on COMmunication Systems NETworkS (COMSNETS), 2020, pp. 519–522. doi:10.1109/COMSNETS48256.2020.9027303.
23. Yildirim, I.; Kilinc, F.; Basar, E.; Alexandropoulos, G.C. Hybrid RIS-Empowered Reflection and Decode-and-Forward Relaying for Coverage Extension. *IEEE Communications Letters* **2021**, *25*, 1692–1696. doi:10.1109/LCOMM.2021.3054819.
24. Zhao, J.; Chen, M.; Chen, M.; Yang, Z.; Wang, Y.; Cao, B.; Shikh-Bahaei, M. Energy Efficient Full-Duplex Communication Systems with Reconfigurable Intelligent Surface. In Proceedings of the 2020 IEEE 92nd Vehicular Technology Conference (VTC2020-Fall), 2020, pp. 1–5. doi:10.1109/VTC2020-Fall49728.2020.9348826.
25. Peng, Z.; Zhang, Z.; Pan, C.; Li, L.; Swindlehurst, A.L. Multiuser Full-Duplex Two-Way Communications via Intelligent Reflecting Surface. *IEEE Transactions on Signal Processing* **2021**, *69*, 837–851. doi:10.1109/TSP.2021.3049652.
26. Odeyemi, K.O.; Owolawi, P.A.; Olakanmi, O.O. Reconfigurable intelligent surface assisted mobile network with randomly moving user over Fisher-Snedecor fading channel. *Physical Communication* **2020**, *43*, 101186.

27. Atapattu, S.; Fan, R.; Dharmawansa, P.; Wang, G.; Evans, J.; Tsiftsis, T.A. Reconfigurable Intelligent Surface Assisted Two–Way Communications: Performance Analysis and Optimization. *IEEE Transactions on Communications* **2020**, *68*, 6552–6567. doi:10.1109/TCOMM.2020.3008402.
28. Boulogeorgos, A.A.A.; Alexiou, A. Performance Analysis of Reconfigurable Intelligent Surface-Assisted Wireless Systems and Comparison With Relaying. *IEEE Access* **2020**, *8*, 94463–94483. doi:10.1109/ACCESS.2020.2995435.
29. Atapattu, S.; Tellambura, C.; Jiang, H. A Mixture Gamma Distribution to Model the SNR of Wireless Channels. *IEEE Transactions on Wireless Communications* **2011**, *10*, 4193–4203. doi:10.1109/TWC.2011.111210.102115.
30. Ben Rached, N.; Kammoun, A.; Alouini, M.S.; Tempone, R. A Unified Moment-Based Approach for the Evaluation of the Outage Probability With Noise and Interference. *IEEE Transactions on Wireless Communications* **2017**, *16*, 1012–1023. doi:10.1109/TWC.2016.2635652.
31. Annamalai, A.; Tellambura, C.; Bhargava, V. Simple and accurate methods for outage analysis in cellular mobile radio systems-a unified approach. *IEEE Transactions on Communications* **2001**, *49*, 303–316. doi:10.1109/26.905889.
32. Editor, G.C.R. Rates of convergence in the central limit theorem. *Advances in Mathematics* **1987**, *66*, 318–318.
33. Raič, M. A multivariate Berry–Esseen theorem with explicit constants. *Bernoulli* **2019**, *25*. doi:10.3150/18-bej1072.
34. Döring, H.; Jansen, S.; Schubert, K. The method of cumulants for the normal approximation. *Probability Surveys* **2022**, *19*, 185 – 270. doi:10.1214/22-PS7.
35. Bickel, P.J.; Robinson, J. Edgeworth Expansions and Smoothness. *Annals of Prob.* **1982**, *10*, 500 – 503. doi:10.1214/aop/1176993873.
36. Bally, V.; Caramellino, L.; Poly, G. Convergence in distribution norms in the CLT for non identical distributed random variables. *Electronic Journal of Probability* **2018**, *23*, 1 – 51. doi:10.1214/18-EJP174.
37. Stewart, M. Fast algorithms for structured matrix computations. *Handbook of Linear Algebra, CRC Press* **2014**.
38. Bobkov, S.G. Asymptotic Expansions for Products of Characteristic Functions Under Moment Assumptions of Non-integer Orders. In Proceedings of the Convexity and Concentration; Carlen, E.; Madiman, M.; Werner, E.M., Eds.; Springer New York: New York, NY, 2017; pp. 297–357.
39. Touchette, H. A basic introduction to large deviations: Theory, applications, simulations, 2011. doi:10.48550/ARXIV.1106.4146.
40. McDonald, D. A Local Limit Theorem for Large Deviations of Sums of Independent, Nonidentically Distributed Random Variables. *The Annals of Probability* **1979**, *7*, 526 – 531. doi:10.1214/aop/1176995052.
41. Petrov, V.V.; Robinson, J. Large Deviations for Sums of Independent Non Identically Distributed Random Variables. *Communications in Statistics - Theory and Methods* **2008**, *37*, 2984–2990. doi:10.1080/03610920802027438.
42. Petrov, V.V. On large deviations of sums of random variables. (Russian). *Vestnik Leningrad Univ. 16* **1961**, pp. 25–37.
43. Wijekoon, V.B.; Viterbo, E.; Hong, Y. Decoding of NB-LDPC Codes Over Subfields. *IEEE Transactions on Communications* **2021**, *69*, 716–727. doi:10.1109/TCOMM.2020.3036073.
44. Bocharova, I.E.; Kudryashov, B.D.; Ovsyannikov, E.P.; Skachek, V. A Random Coding Bound on the ML Decoding Error Probability for NB LDPC Coded QAM Signals. In Proceedings of the 2021 IEEE Information Theory Workshop (ITW), 2021, pp. 1–6. doi:10.1109/ITW48936.2021.9611390.
45. Abbasi, F.; Mahdavifar, H.; Viterbo, E. Hybrid Non-Binary Repeated Polar Codes. *IEEE Transactions on Wireless Communications* **2022**, pp. 1–1. doi:10.1109/TWC.2022.3159807.
46. Falk, M.; Bauch, G.; Nissen, I. Analysis of Non-binary Polar Codes over GF(3) and GF(5) with Phase Shift Keying for Short Messages. In Proceedings of the 2020 IEEE 92nd Vehicular Technology Conference (VTC2020-Fall), 2020, pp. 1–5. doi:10.1109/VTC2020-Fall49728.2020.9348796.